Removal of basic yellow cationic dye by an aqueous dispersion of Moroccan stevensite

Mohamed Ajbary[1], Alberto Santos[1], Victor Morales-Flórez[2,3*], Luis Esquivias[2,3]

[1]Departamento de Ciencias de la Tierra, Universidad de Cádiz, Puerto Real, 11510 Cádiz, Spain.

[2]Instituto de Ciencia de Materiales de Sevilla, ICMS (CSIC-US), Av. Américo Vespucio 49, 41092, Seville, Spain.

[3]Departamento de Física de la Materia Condensada, Universidad de Sevilla. Av. Reina Mercedes s/n, 41012, Seville, Spain.

* To whom correspondence should be addressed.

Abstract

The aim of this study was to investigate the adsorption of basic yellow, a cationic dye, from aqueous solution by natural stevensite, with 104 m^2/g of specific surface area. The kinetics and the effects of several experimental parameters such as the pH of the solution, adsorbent dose and initial dye concentration were researched using a batch adsorption technique. The results showed that an alkaline pH favoured basic yellow adsorption and the adsorption reached equilibrium in about 20 min. It was concluded that the adsorption process was governed by the electrostatic interaction. The isothermal data were fitted by means of Langmuir and Freundlich equations, and a monolayer adsorption capacity of 454.54 mg/g was calculated. Finally, a good agreement was found between the pseudo-second order model and the experimental data. A high maximum adsorption capacity was obtained (526 mg/g)

and a maximum surface density of ~9 dye molecules/nm^2 was estimated, involving a columnar arrangement of the adsorbed molecules.

Keywords: Adsorption kinetics; basic yellow; cationic dye; stevensite; wastewater;

1. Introduction

There are more than 100,000 commercially available dyes with over 7×10^5 t of dyes produced annually (Zollinger, 1987). It is estimated that 2% of them are discharged in effluent from manufacturing operations, while 10% are discharged from textile and associated industries (Easton, 1995). Even in small amounts, they are highly visible and have undesired effects to the environment. Furthermore, most dyestuffs are stable to light and oxidation (Namasivayam et al., 2002; Mátivier-Pignon et al., 2003; Orthman et al., 2003; Waranusantigul et al., 2003).

The removal of low levels of such compounds is difficult. Several treatment methods have been developed for decontamination purposes including coagulation, chemical oxidation, membrane separation, electrochemical processes, and adsorption techniques. The last one has been recognised as a cost-effective process to remove dyes from aqueous solution and it has been tested with many adsorbents; activated carbon has been the most commonly used adsorbent because of its high adsorption capacity. However, the operating cost of activated carbon adsorption is high (McKay, 1983; Leyva-Ramos, 1989; Tsai et al., 2001; Pendleton and Wu, 2003; Singh et al., 2003), though some strategies to reduce costs were also proposed (Kannan and Sundaram, 2001). Problems of regeneration and difficulty in separation from the wastewater after use are the two major concerns of using this material. Other commonly-used adsorbents are chitin (McKay et al., 1983), fly ash (Gupta et al.,

1988), silica gels (Ahmed and Ram, 1992), peat (Allen, 1996; Ho and McKay, 1998), and more recently, heteropoly blue-intercalated layered double hydroxide (Bi et al., 2011). A wide compilation of the different considered strategies can be found in a review of Forgacs et al. (2004). However, the amount of adsorbed dye by these methods is not very high. To improve the efficiency of the adsorption processes, it is essential to develop more effective and cheaper adsorbents.

Clay minerals have a great potential to fix pollutants such as heavy metals, dye wastewater and organic compounds, and they are widely applied in many fields of science and technology, for example, for the removal of liquid impurities and the purification of gases with surfactant-modified montmorillonite as adsorbent agent (Juang et al., 2002), or the dyes and surfactants from tannery waste waters with natural and acid-activated bentonite and sepiolite (Espantaleón et al., 2003). Kaolin has also been considered for cationic dyes removal from aqueous solutions (Nandi et al., 2009). The porous structure of clay minerals can adsorb large amounts of colorant wastes and their use is justified by low cost, high specific surface area (SSA) and structural properties. Recent studies have been devoted to the mineralogical characterisation of stevensite from the Atlas Mountains of Morocco (called locally "Ghassoul" or "Rhassoul") and its possible applications in the water treatment field (Elmchaouri and Mahboub, 2005; Benhammou et al., 2005; Bouna et al., 2010; Elass et al., 2011). SSA of 150 m^2/g and 134 m^2/g, and adsorption capacities from 240 mg/g up to 600 mg/g were previously reported.

The objective of this work was to examine the effectiveness of this abundant stevensite material in the removal of basic dyes. Basic yellow (BY) (Wu et al., 2011) was selected as the modelled basic dye for this work. It is a dyestuff with

$C_{15}H_{19}N_3O_4S$ as its molecular formula (M.W.: 337.4 g/mol), and its chemical name is 1-methyl-4-((methylphenylhydrazono) methyl) pyridinium methylsulphate.

2. Experimental

2.1. Sampling

The clay mineral was extracted from the Ghassoul mountains (Millot, 1954) and was considered as stevensite, or magnesian smectite (Caillère et al., 1982; Benhammou et al., 2009). The raw clay sample was crushed, ground, sieved through a 200 μm sieve, and dried at 110°C in an oven for 2 h before use. Its chemical composition was determined by X-ray fluorescence (Philips PW 1666) spectroscopy. X-ray diffraction (XRD) experiments were performed using a Bruker diffractometer (D8 Advance) with a graphite monochromator and Cu Kα radiation. The intensities were measured in a 2Θ range (3°–60°) with a step of 0.02° and a counting time of 5 s per step. Physisorption experiments were performed in a Micromeritics device model ASAP2010 at a constant temperature of 77.35 K. Samples were degasified at 150ºC under vacuum for 2 h prior to the experiment. The SSA and the pore size distribution were determined by the Brunauer–Emmett–Teller (BET) method and the Barret-Joyner-Hallenda (BJH) method, respectively.

2.2. Adsorption tests

Adsorption tests were carried out in a discontinuous reactor at room temperature, using a volume V = 50 ml of distilled water, containing the adsorbent material and the dye. The effect of the adsorbent dosage (m/V, where m is the adsorbent mass), the initial pH and the initial concentration of the dye on adsorption

(C_0) were studied separately. The mixture was constantly stirred for a period of time fixed by kinetic tests and then filtered (0.45 μm cellulose nitrate filters, Sartorius).

The equilibrium concentration (*Ce*) was determined using a UV-visible spectrophotometer (JENWAY UV/VIS spectrophotometer model 6505) at the maximum absorbance wavelength (λ_{max} = 412 nm). The amount of metal adsorbed per unit mass of adsorbent, or adsorption capacity, was calculated as:

$$q_e = (C_0 - C_e) \times \frac{V}{m} \qquad (1)$$

The pH of the solution was adjusted by adding 0.1M HNO_3 or 0.1M NaOH solution as required. Blank tests (without dye) were done for each series of experiments as a reference. All experiments were performed twice.

3. Results and discussion

The chemical composition of the analysed stevensite-rich sample is summarized in Table 1. These results confirm the magnesium silicate nature of this mineral, with a maximum Mg/Si molar ratio of 0.83. Very low concentrations of Fe or Ca were also detected and Na was not detected in this analysis. The X-ray diffraction pattern showed that Mg-rich trioctahedral smectite, stevensite-15A, was the dominant phase, and minor proportions included reflections of quartz-α and dolomite (Fig. 1). Moreover, the presence of reflections corresponding to other minerals from the smectite group (montmorillonite, PDF files 00-011-0303 and 00-012-0219) was detected.

The analysis of the microstructure by nitrogen physisorption reveals the existence of channel-like pores (Kruk and Jaroniec, 2001). The calculated SSA S_{BET} = 104 m^2/g, is roughly lower than those previously reported (Benhammou et al., 2005; Bouna et al., 2010; Elass et al., 2011), but almost an order of magnitude higher than

other considered adsorbents as kaolin, for example (Nandi, et al., 2009). The BJH analysis yielded a well defined typical pore size of 3.9 nm.

Table 1.

Fig. 1.

3.1. Effect of adsorbent dose (m/V)

In Fig. 2a, the amount of BY removed for a constant dye concentration C_0 = 1 g/l and different adsorbent doses is shown. It can be seen that this amount increased up to total adsorption. Obviously, the presence of more adsorption sites with higher adsorbent dosage allows the increase of the amount of removed dye. But raising adsorbent dose above 2 g/l, the increment of dye removal was very low until all the dye was removed (e.g. 99.96% of removal for adsorbent dose = 3 g/l).

Fig. 2.

3.2. Effect of initial pH

The pH is the most important factor affecting the adsorption process. To study the influence of pH on the adsorption capacity of stevensite, experiments were performed with the initial pH varying from 2 to 11, for C_0 = 1 g/l and adsorbent dose = 1.0 g/l. The results of the pH effect on the adsorption of BY onto stevensite are shown in Fig. 2b. It can be seen that the BY dye removal increased from 2 to 7 and then the removal remained almost the same at pH > 7. Two possible mechanisms of BY adsorption by the stevensite may be considered: electrostatic interactions between

148 the surface groups of stevensite and the cationic dye, and a chemical reaction between
149 the adsorbate and the adsorbent. At pH > 7, a significantly high electrostatic attraction
150 existed between the negatively charged surface of the adsorbent and the cationic dye.
151 As long as the pH of the system decreased, the number of positively charged sites
152 increased, and the number of negatively charged sites decreased. Negatively charged
153 sites on the adsorbent surface favoured the adsorption of cationic dye due to this
154 interaction. On the other hand, the lower adsorption of BY at pH < 7 was due to the
155 presence of excess H^+ competing with the cationic dye for adsorption sites. This
156 suggests that the first mechanism, i.e. electrostatic interactions, might be operative.
157
158 *3.3. Kinetic study and effect of initial concentration of the dye*
159 The kinetics and the effect of initial dye concentration on the removal of dye
160 by stevensite are presented in Fig. 3. The adsorption capacity with initial adsorbent
161 concentration = 1 g/l increased with increasing time, attaining equilibrium after
162 approximately 20 min, independently of the initial dye concentration used in this
163 study (C_0 = 0.25 g/l, C_0 = 0.50 g/l and C_0 = 1.0 g/l).
164 The three kinetic curves follow a saturation-like behaviour, being the
165 characteristic time independent of the dye initial concentration C_0. On the other hand,
166 an increase in the initial dye concentration led to an increase in the adsorption
167 capacity within the studied range. As the initial dye concentration increased from 0.25
168 g/l to 1.0 g/l, the maximum adsorption capacity of the dye onto the clay changed from
169 249 mg/g to 506 mg/g. This maximum value of 506 mg/g is significantly higher than
170 other reported adsorption capacity values for BY onto MCM41 or MCA (Wu et al.,
171 2011), or onto modified montmorillonite and other clay minerals (Turabik, 2008;
172 Monvisade and Siriphannon, 2009; Kaemkit et al., 2012).

At the same time, the obtained adsorption capacity value is also higher that those reported for other anionic and cationic dyes onto stevensite, for example, orange G (Bouna et al., 2010), methylene blue (Bouna et al., 2010, Elass et al., 2010) or malachite green (Karim et al., 2011), or even for other dyes onto kaolin (Nandi et al., 2009), activated carbon (Kannan and Sundaram, 2001) or montmorillonite (Almeida et al., 2009). However, a roughly higher adsorption capacity value is reported for methyl violet onto stevensite (Elass et al., 2011).

Different factors may be responsible for the better performance found for BY onto stevensite in comparison to other adsorbents, or for other dyes onto stevensite. In the first case, the differences found in the nature and physicochemical properties as SSA of the adsorbents can explain this phenomenon, revealing the natural untreated stevensite as one of the best adsorbents. In the second case, the adsorption mechanism discriminates anionic dyes as the orange G against the cationic dyes for adsorption on the negatively charged surface of the stevensite (Bouna et al., 2010). Among cationic dyes, features of the adsorbents as purity, homogeneity and SSA would influence the surface charge density available for dye adsorption and consequently the adsorption capacity.

Fig. 3.

3.4. Isotherm studies

BY adsorption isotherm data for different initial dye concentrations were investigated to fit the Langmuir and Freundlich models. These data were obtained by dye concentration measurements after adsorbent/adsorbate contact periods equal to the equilibrium time.

$$\frac{Ce}{q_e} = \frac{1}{q_{\max} K_L} + \frac{Ce}{q_{\max}} \qquad (2)$$

where q_e is the equilibrium dye concentration on the adsorbent (mg/g), *Ce* is the equilibrium dye concentration in solution (mg/l), q_{max} is the monolayer capacity of the adsorbent (mg/g) and K_L is the Langmuir adsorption constant (l/mg) (Langmuir, 1918). A plot of Ce/q_e versus *Ce* (Fig. 4, top) gave a straight line for the slope $1/q_{max}$ and intercepted the ordinate axis at $1/q_{max}K_L$. The Langmuir equation is applicable to systems where homogeneous adsorption occurs; this means that the adsorption of each adsorbate molecule onto the surface has equal adsorption activation energy (Juang et al., 1997).

On the other hand, the Freundlich equation is

$$\ln q_e = \ln K_F + \frac{1}{n} \ln C_e \qquad (3)$$

where q_e is the equilibrium dye concentration on the adsorbent (mg/g), *Ce* is the equilibrium dye concentration in solution (mg/l), and K_F (l/g), the Freundlich constant and *n,* the adsorption intensity, are characteristic parameters of the system, related with the adsorption capacity and surface heterogeneity, respectively. The Freundlich equation is employed to describe heterogeneous systems and reversible adsorption and is not restricted to monolayer formation (Freundlich, 1906). A plot of $ln(q_e)$ vs. *ln(Ce)* for the adsorption of BY onto clay (Fig. 4, bottom) was employed to generate the ordinate K_F and the slope $1/n$.

In addition, the other Freundlich constant ($1/n$) is also a measure of the adsorption deviation from linearity. If *n* is equal to unity, the adsorption is linear. This means that the adsorption sites are homogeneous (as in the Langmuir model) in energy and no interaction takes place between the adsorbed species. In the case $1/n < 1$, which indicates favourable adsorption, the adsorption capacity increases and new adsorption sites appear. When $1/n > 1$, the adsorption bond becomes weak;

222 unfavourable adsorption takes place as a result of the diminution in adsorption
223 capacity (Jiang et al., 2002; Tsai et al., 2003).
224
225 **Fig. 4**
226
227 The values of q_{max}, K_L, K_F, and $1/n$ and the correlation coefficients for
228 Langmuir (R^2_L) and for Freundlich (R^2_F) models are given in Table 2, and the linear
229 fittings are plotted in Fig. 4. The values of the correlation coefficients showed an
230 almost perfect agreement between the experimental data and both models. The
231 correlation coefficient close to 1 for the Langmuir model indicates that the adsorption
232 took place in the interlayer pores. Moreover, the values of $1/n$ for stevensite were < 1,
233 which indicates that adsorption processes are favourable and high adsorption took
234 place.
235 The adsorption of the dye was characterized by the calculated Langmuir
236 monolayer capacity value q_{max} = 454.54 mg/g. In Fig. 3, the value of the monolayer
237 capacity q_{max} is indicated by a dashed line for comparison purposes. Comparing this
238 value with the experimental saturation values for different dye concentrations, it can
239 be inferred that for low dye concentrations (< 0.50 g/l), a complete monolayer is not
240 formed (saturated value below the theoretical monolayer adsorption capacity),
241 whereas for 0.5 g/l, the adsorption could be described as the complete monolayer
242 formation. Moreover, the 1.0 g/l experiment corroborates the appearance of new
243 adsorption sites, above the monolayer theoretical capacity, in coherence with the $1/n$ <
244 1 obtained from the Freundlich model. In summary, these values confirm that
245 stevensite has a high affinity for dye removal.
246

247 **Table 2.**

248

249 *3.5. Adsorption kinetic study*

250 In order to investigate the adsorption processes of BY on stevensite, several
251 simplified kinetic models, namely pseudo-first-order and pseudo-second-order, were
252 considered. The pseudo-first-order kinetic model (Lagergren, 1898) can be expressed
253 as:

254 $$\frac{dq_t}{dt} = k_F(q_e - q_t) \qquad (4)$$

255 where q_t is the amount of adsorbate adsorbed in time t (mg/g), q_e is the adsorption
256 capacity at equilibrium (mg/g), k_F is the pseudo-first-order rate constant (min^{-1}), and t
257 is time (min). The integration of Eq (4) for the boundary conditions, q_t=0 to q_t and t=0
258 to t, results in:

259 $$\log(q_e - q_t) = \log q_e - \frac{k_F}{2.303}t \qquad (5)$$

260 The values of the adsorption rate constant (k_F) for BY adsorption on stevensite
261 were determined from linear fitting of the experimental values of $log\ (q_e\text{-}q_t)$ vs. t. The
262 best description of the adsorption kinetics was obtained by the pseudo-first-order
263 model for the first 30 min; thereafter, the data departed from theory. Thus, the model
264 represents the initial stages where rapid adsorption occurs but cannot be applied for
265 the entire adsorption range (McKay and Ho, 1999). This confirms that the pseudo-
266 first-order model does not adequately describe the adsorption kinetics for BY by
267 stevensite. The calculated parameters are presented in Table 3.

268 According to Ho and McKay (1999), the pseudo-second-order model (Eq (6))
269 agrees with the complexation reaction:

$$\frac{dq_t}{dt} = k_s (q_e - q_t)^2 \qquad (6)$$

where k_s (g/mg·min) is the pseudo-second-order rate constant. Integrating and noting that $q_t = 0$ at $t = 0$, results in:

$$q_t = \frac{t}{\frac{1}{k_s q_e^2} + \frac{t}{q_e}} \qquad (7)$$

The linear form of which is:

$$\frac{t}{q_t} = \frac{1}{k_s q_e^2} + \frac{1}{q_e} t \qquad (8)$$

The initial adsorption rate, h (mg/g·min), is defined as:

$$h = k_s q_e^2 \qquad (9)$$

Then, Eqs (7) and (8) become

$$q_t = \frac{t}{\frac{1}{h} + \frac{t}{q_e}} \qquad (10)$$

and

$$\frac{t}{q_t} = \frac{1}{h} + \frac{1}{q_e} t \qquad (11)$$

Table 3 abridges the results of the constant rate calculations for different initial dye concentrations according to the pseudo-second-order and pseudo-first-order adsorption models, and both linear fittings of t/q_t vs. t are plotted in Fig. 5.

Fig. 5.

A good fitting of this kinetic model (continuous lines in Fig. 3) with the experimental data is obtained. These facts suggest that the pseudo-second-order

adsorption mechanism was predominant, similar to what was previously proposed for crystal violet and brilliant green adsorption in kaolin (Nandi et al., 2009).

Table 3.

Finally, if we consider the maximum adsorption capacity estimated by the fitting, that is, q_e = 526 mg/g and the SSA of the adsorbent (104 g/m^2), we can conclude the maximum surface dye density obtained is 5.06 mg/m^2, or ~9 BY molecules/nm^2. Considering the proposed BY molecule size of 1.4 nm x 0.7 nm x 0.4 nm (Wu et al., 2011), a columnar arrangement of the adsorbed dye cations surrounding the surface of the stevensite is concluded.

4. Conclusions

The high efficiency of the natural raw stevensite for the cationic dye basic yellow 87 removal from an aqueous solution was confirmed. Adsorption equilibrium was practically achieved within 20 min, being this equilibrium time independent of the dye concentration. The adsorption capacity was affected by the initial dye concentration; the uptake increased with increasing initial dye concentration, above the monolayer adsorption capacity derived from Langmuir isotherm model. The Freundlich model confirmed that adsorption processes of basic yellow on stevensite were favourable, and adsorption sites appeared above the Langmuir theoretical monolayer capacity. In addition, the adsorption is governed by the electrostatic interaction between negatively sites of stevensite and cationic dye, and therefore it is favoured by alkaline pH. Finally, the pseudo-second-order kinetic model was

315 successfully fitted to the kinetic studies, and a very high adsorption capacity of 526
316 mg/g of basic yellow onto stevensite was measured.
317
318 **Acknowledgements**
319 The authors would like to acknowledge the research services of the ICMS (CSIC-US),
320 especially to I. Rosa Cejudo for her help on the physisorption experiments. This work
321 was possible thanks to the support of the Agencia Española de Cooperación
322 Internacional (AECI), project number A/018025/08, within the framework of
323 "Programa de Cooperación Interuniversitaria PCI-Mediterráneo". The authors are also
324 grateful to the Consejería de Innovación Ciencia y Empresa of the Junta de Andalucía
325 (Spain) for supporting this work with the annual Grant TEP115. VMF would like to
326 thank the JAE-Doc program from the CSIC.
327
328 **References**
329 Ahmed, M.N., Ram, R.N., 1992. Removal of basic dye from waste-water using silica
330 adsorbent. Env. Pollut. 77, 79-86.
331 Allen, S.J., 1996. Types of adsorbent materials. In: McKay, G. (Ed.), C.R.C, Boca
332 Raton (USA), pp. 59–97.
333 Almeida, C.A.P., Debacher, N.A., Downs, A.J., Cottet, L., Mello, C.A.D., 2009.
334 Removal of methylene blue from colored effluents by adsorption on
335 montmorillonite clay. J. Colloid. Interface Sci. 332(1), 46-53.
336 Benhammou, A., Yaacoubi, A., Nibou, L., Tanouti, B., 2005. Adsorption of metal
337 ions onto Moroccan stevensite: kinetic and isotherm studies. J. Colloid Interface
338 Sci. 282, 320–326.

339 Benhammou, A., Tanouti, B., Nibou, L., Yaacoubi, A., Bonnet, J.P., 2009.
340 Mineralogycal and physicochemical investigation of Mg-smectite from Jbel
341 Ghassoul, Morocco. Clays Clay Miner. 57(2), 264-270.
342 Bi, B., Xu, L., Xu, B., Liu, X., 2001. Heteropoly blue-intercalated layered double
343 hydroxides for cationic dye removal from aqueous media. Appl. Clay Sci. 54,
344 242–247.
345 Bouna, L., Rhouta, B., Amjoud, M., Jada, A., Maury, F., Daoudi, L., Senoq, F., 2010.
346 Correlation between eletrokinetic mobility and ionic dyes adsorption of
347 Moroccan stevensite. Appl. Clay Sci. 48, 527-530.
348 Caillère, S., Henin, S., Rautureau, M., 1982. Minéralogie des Argiles: Classification et
349 Nomenclature. V. 2. (Eds) Masson et INRA, Paris, p 189.
350 Easton, J.R., 1995. In: Cooper P (Ed.), Colour in Dye house Effluent, The Alden
351 Press, Oxford.
352 Elass, K., Laachach, A., Alaoui, A., Azzi, M., 2010. Removal of methylene blue from
353 aqueous solution using ghassoul, a low-cost adsorbent. Appl. Ecol. Environ.
354 Res. 8(2), 153-163.
355 Elass, K., Laachach, A., Alaoui, A., Azzi, M., 2011. Removal of methyl violet from
356 aqueous solution using a stevensite-rich clay from Morocco. Appl. Clay Sci. 54,
357 90-96.
358 Espantaleón, A.G., Nieto, J.A., Fernández, M., Marsal, A., 2003. Use of activated
359 clays in the removal of dyes and surfactants from tannery waste waters. Appl.
360 Clay Sci. 24, 105-110.
361 Elmchaouri, A., Mahboub, R., 2005. Effects of preadsorption of organic amine on Al-
362 PILCs structures. Colloids Surf, A. Physicochem. Eng. Asp. 259, 135–141.

363 Forgacs, E., Cserhati, T., Oros, G., 2004. Removal of synthetic dyes from
364 wastewaters: a review. Environ. Int. 30, 953-971.
365 Freundlich, H. M.F., 1906. Over the adsorption in solution. J. Phys. Chem. 57, 385-
366 470.
367 Gupta, G.S., Prasad, G., Panday, K.K., Singh V.N., 1988. Removal of chrome dye
368 from aqueous solutions by fly ash. Water Air Soil Pollut. 37, 13-24.
369 Ho, Y.S., McKay, G., 1998. Sorption of dye from aqueous solution by peat. Chem.
370 Eng. J. 70 (2), 115-124.
371 Ho, Y.S., McKay, G., 1999. Pseudo-second order model for sorption processes.
372 Process Biochem. 34, 451-465.
373 Jiang, J-Q., Cooper, C., Ouki, S., 2002. Comparison of modified montmorillonite
374 adsorbents Part I: preparation, characterization and phenol adsorption.
375 Chemosphere 47, 711-716.
376 Juang, R.S., Lin, S.H., Tsao, K.H., 2002. Mechanism of the sorption of phenols from
377 aqueous solutions onto surfactant-modified montmorillonite. J. Colloid Interface
378 Sci. 254, 234–241.
379 Juang, R.S., Tseng, R.L., Wu, F.C., Lee, S.H., 1997. Adsorption behaviour of reactive
380 dyes from aqueous solutions on chitosan. J. Chem. Technol. Biotechnol. 70,
381 391-399.
382 Kaemkit, C., Monvisade, P., Siriphannon, P., Nukeaw, J., 2012. Water-soluble
383 chitosan intercalated montmorillonite nanocomposites for removal of basic blue
384 66 and basic yellow from aqueous solution. J. Appl. Polym. Sci. 128(1), 879-
385 887.

386 Kannan, N., Sundaram, M.M., 2001. Kinetics and mechanism of removal of
387 methylene blue by adsorption on various carbons—a comparative study. Dyes
388 and Pigments 51, 25–40.
389 Karim, A.B., Mounir, B., Hachkar, M., Bakasse, M., Yaacoubi, A., 2011. Adsorption
390 of Malachite Green dye onto raw Moroccan clay in batch and dynamic system.
391 Can. J. Environ. Construc. Civil Eng. 2(2), 5-13.
392 Kruk, M., Jaroniec, M., 2001. Gas Adsorption Characterization of Ordered Organic-
393 Inorganic Nanocomposite Materials. Chem. Matter. 13, 3169-3183.
394 Lagergren, S., 1898. Zur theories der sogenannten adsorption gelöster stoffe,
395 Kungliga. Svenska Vetenskapsakademiens. Handlingar, Band 24, No. 4, 1-39.
396 Langmuir, I., 1918. The adsorption of gases on plane surfaces of glass, mica and
397 platinum. J. Am. Chem. Soc. 40, 1361-1403.
398 Leyva-Ramos, R., 1989. Effect of temperature and pH on the adsorption of an anionic
399 detergent on activated carbon. J. Chem. Tech. Biotechnol. 45, 231–240.
400 Mátivier-Pignon, H., Faur-Brasquet, C., Le Cloirec, P., 2003. Adsorption of Dyes
401 onto Activated Carbon Cloths: Approach of Adsorption Mechanisms and
402 Coupling of ACC with Ultrafiltration to Treat Coloured Wastewaters. Sep.
403 Purif. Technol. 31, 3-11.
404 McKay, G., 1983. The adsorption of dyestuffs from aqueous solutions using activated
405 carbon: external mass transfer processes. J. Chem. Tech. Biotechnol. 33A, 205–
406 218.
407 McKay, G., Ho, Y. S., 1999. The sorption of lead(II) ions on peat. Water. Res. 33,
408 578-584.
409 McKay, G., Blair, H.S., Gardner, J.R., 1983. Rate studies for the adsorption of
410 dyestuffs onto chitin. J. Colloid Interface Sci. 95, 108–119.

411 Millot, G., 1954. La Ghassoulite, pole magnésien de la série des montmorillonite.
412 Comptes Rendus Acad. Sci., Paris, 371–382.
413 Monvisade, P., Siriphannon, P., 2009. Chitosan intercalated montmorillonite:
414 Preparation, characterization and cationic dye adsorption. Appl. Clay Sci. 42,
415 427-431.
416 Namasivayam, C., Yamuna, R.T., Arasi, D.J.S.E., 2002. Removal of procion orange
417 from wastewater by adsorption on waste red mud. Sep. Sci. Technol. 37(10),
418 2421-2431.
419 Nandi, B.K., Goswami, A., Purkait, M.K., 2009. Removal of cationic dyes from
420 aqueous solutions by kaolin: Kinetic and equilibrium studies. Appl. Clay Sci.
421 42, 583-590.
422 Orthman, J., Zhu, H.Y., Lu, G.Q., 2003. Use of anion clay hydrotalcite to remove
423 colored organics from aqueous solutions. Sep. Purif. Technol. 31, 53-59.
424 Pendleton, P., Wu, S.H., 2003. Kinetics of dodecanoic acid adsorption from caustic
425 solution by activated carbon. J. Colloid Interface Sci. 266, 245–250.
426 Singh, K.P., Mohan, D., Sinha, S., Tondon, , Gosh, D., 2003. Color removal from
427 wastewater using low-cost activated carbon derived from agricultural waste
428 material. Ind. Eng. Chem. Res. 42, 1965–1976.
429 Turabik, M., 2008. Adsorption of basic dyes from single and binary component
430 systems onto bentonite: Simultaneous analysis of Basic Red 46 and Basic
431 Yellow 28 by first order derivative spectrophotometric analysis method. J.
432 Hazard. Mater. 158, 52-64.
433 Tsai, W.T., Lai, C.W., Hsien, K.J., 2003. Effect of particle size of activated clay on
434 the adsorption of paraquat from aqueous solution. J. Colloid Interface Sci. 263,
435 29-34.

436 Tsai, W.T., Chang, C.Y., Lin, M.C., Chien, S.F., Sun, H.F., Hsieh, M.F., 2001.
437 Adsorption of acid dye onto activated carbons prepared from agricultural waste
438 bagasse by $ZnCl_2$ activation. Chemosphere 45, 51–58.
439 Waranusantigul, P., Pokethitiyook, P., Kruatrachue M., Upatham, E.S., 2003. Kinetics
440 of basic dye (methylene blue) biosorption by giant duckweed (Spirodela
441 polyrrhiza). Environ. Pollut. 125, 385-92.
442 Wu, X., Hui, K.N., Hui, K.S., Lee, S.K., Zhoud, W., Chen, R., Hwang, D.H., Cho,
443 Y.R., Son, Y.G., 2011. Adsorption of basic yellow 87 from aqueous solution
444 onto two different mesoporous adsorbents. Chem. Eng. J. 180, 91-98.
445 Zollinger, H., 1987. Color chemistry synthesis, properties and applications of organic
446 dyes and pigments. VCH Publishers, New York, pp 92-102.
447
448
449

450 Table captions

451

452 Table 1. Chemical composition of clay.

453 Table 2. The Langmuir and Freundlich fitting parameters for the adsorption of BY

454 by stevensite.

455

456 Table 3. Pseudo-first-order and pseudo-second-order adsorption parameters of BY

457 dye. Pseudo-second-order function can be plotted and compared with experimental

458 results in Fig. 3.

459

460 Figure captions

461 Fig. 1. X-ray diffraction pattern of natural stevensite. Black line was obtained by
462 smoothing original data (gray line). S: stevensite-15A (PDF: 00-025-1498); Q: quartz-
463 α (PDF: 01-089-8936); D: dolomite (PDF: 01-083-1530).

464

465 Fig. 2. a) Effect of adsorbent dose on the adsorption of BY dye by stevensite; b)
466 Effect of pH on the adsorption of BY dye by stevensite. Lines are guides for the eye
467 only.

468

469 Fig. 3. Variation of adsorption capacity with time, for three different initial dye
470 concentrations. The calculated value of monolayer capacity of the Langmuir
471 adsorption model q_{max} is indicated by a dashed line (see discussion in section
472 3.4). Solid lines are fittings of the simplified kinetic the pseudo-second-order
473 model, as obtained in section 3.5.

474

475 Fig. 4. Top: Langmuir plot and linear fitting for the adsorption of BY onto stevensite;
476 q_e and *Ce* were considered in mg/l and g/l, respectively. Bottom: Freundlich plot and
477 linear fitting for the adsorption of BY onto stevensite. Red lines are linear fittings.

478

479 Fig. 5. Pseudo-second-order kinetic plots for the experimental data shown in Fig. 3.

Table 1

Elements	Percentage present (~~wt~~mass~~.~~ %)
SiO_2	57.94
Al_2O_3	1.47
Fe_2O_3	0.43
MgO	32.46
CaO	0.34
Loss of ignition	7.36

Table 2

Click here to download Table: Table2_err.doc

Langmuir			Freundlich		
q_{max} (mg/g)	K_L (ml/mg)	R^2_L	1/n	K_F (l/g)	R^2_F
455±2	210±9	0.9993	0.64±0.03	81.5±0.6	0.9913

Table 3

Click here to download Table: Table3_err.doc

Initial dye concentration C_0 (mg/l)	Pseudo-first-order			Pseudo-second-order			
	$q_{e,F}$ (mg/g)	k_F (10^{-3} min)	R_F^2	$q_{e,s}$ (mg/g)	k_s (10^{-3} min)	h (mg/g.min)	R_s^2
250	200±10	180±10	0.78	250±3	3.8±0.2	238±9	0.999
500	290±10	120±10	0.95	454±4	1.6±0.1	330±10	0.999
1000	280±30	130±20	0.83	526±4	2.40±0.07	670±10	0.999

Figure 1

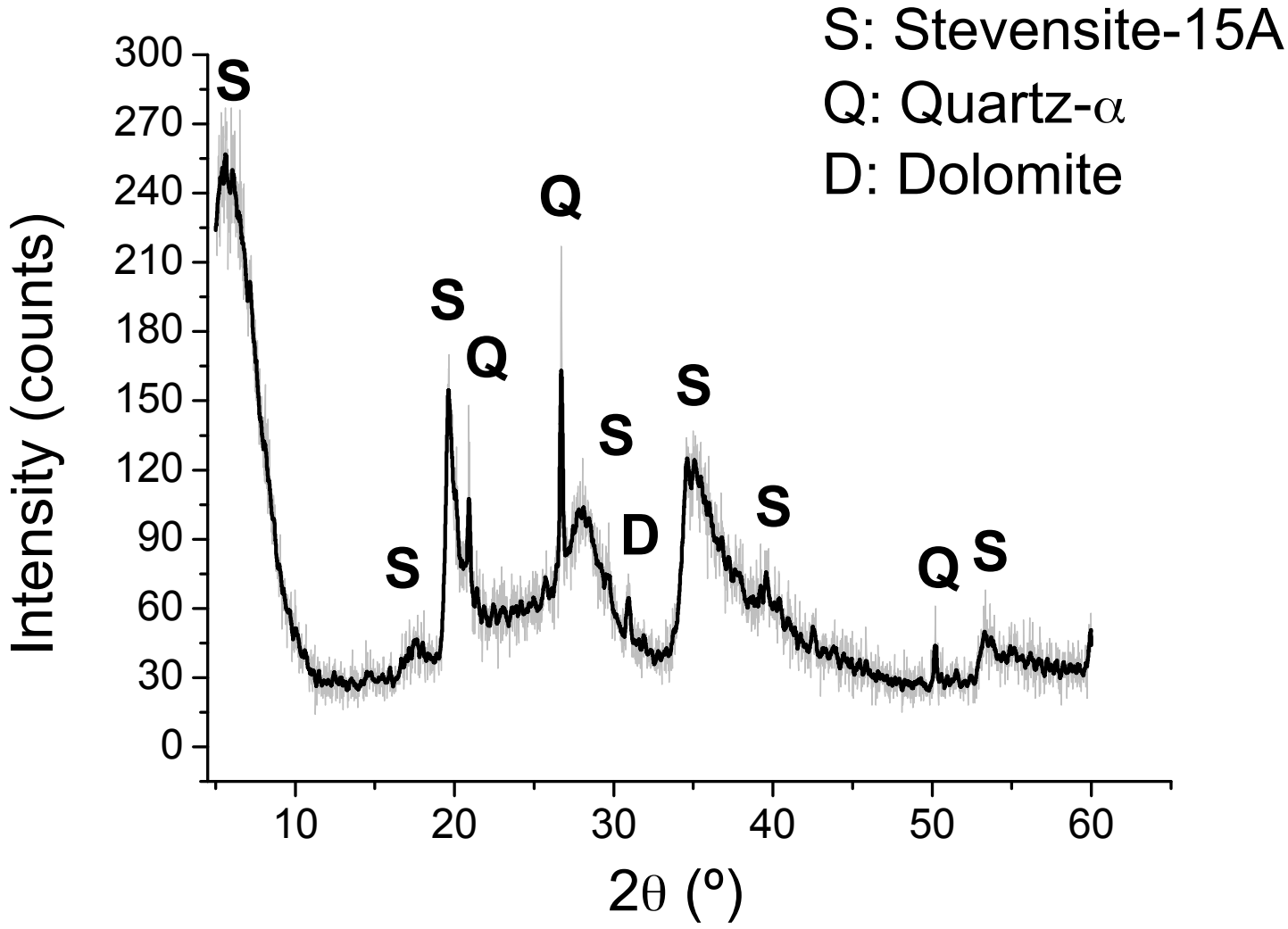
S: Stevensite-15A
Q: Quartz-α
D: Dolomite
Intensity (counts)
2θ (º)
0
30
60
90
120
150
180
210
240
270
300
10
20
30
40
50
60
S
S
Q
Q
S
D
S
S
Q
S

Figure 2

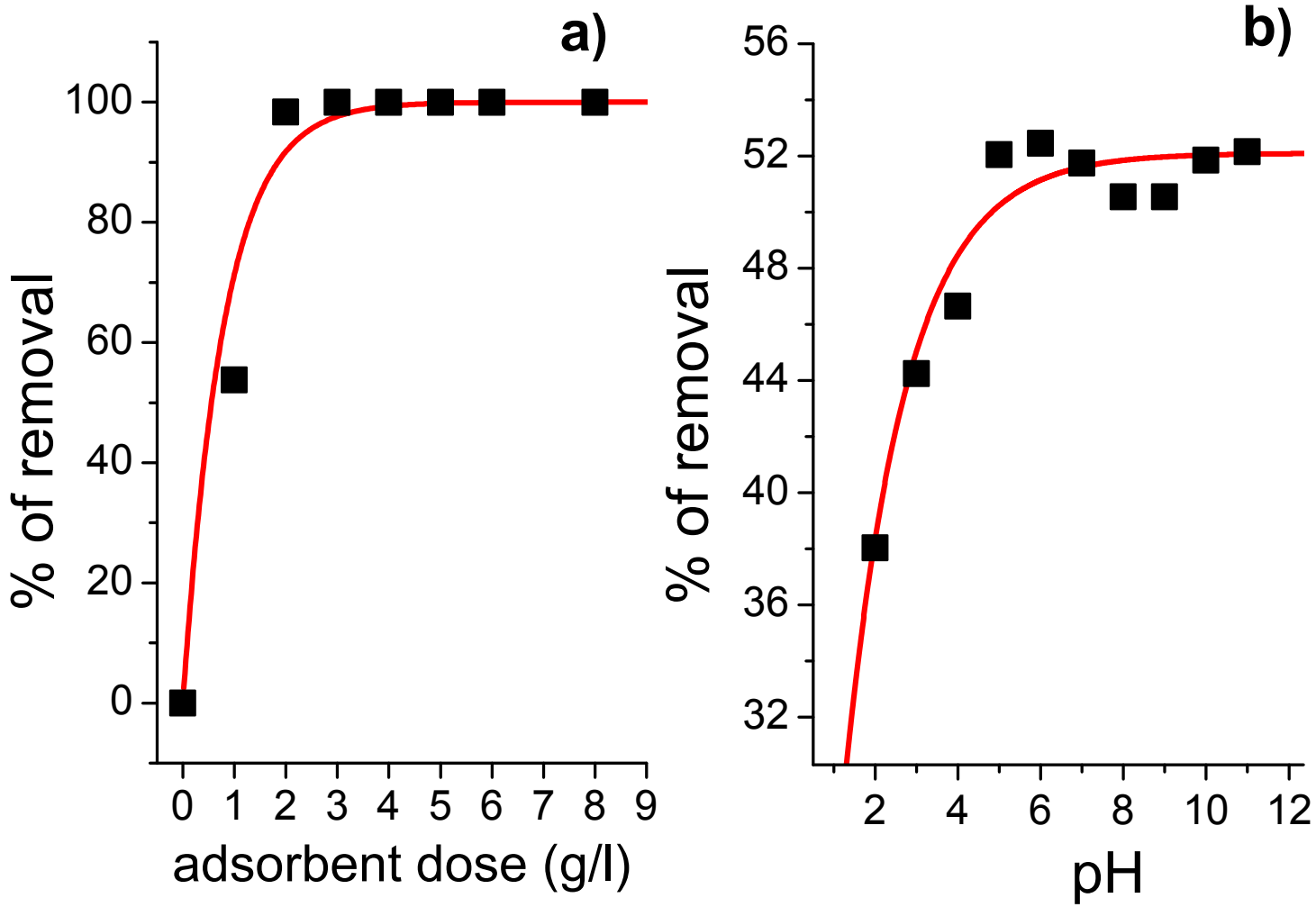
a)
% of removal
100
80
60
40
20
0
0 1 2 3 4 5 6 7 8 9
adsorbent dose (g/l)
b)
% of removal
56
52
48
44
40
36
32
2 4 6 8 10 12
pH

Figure 3

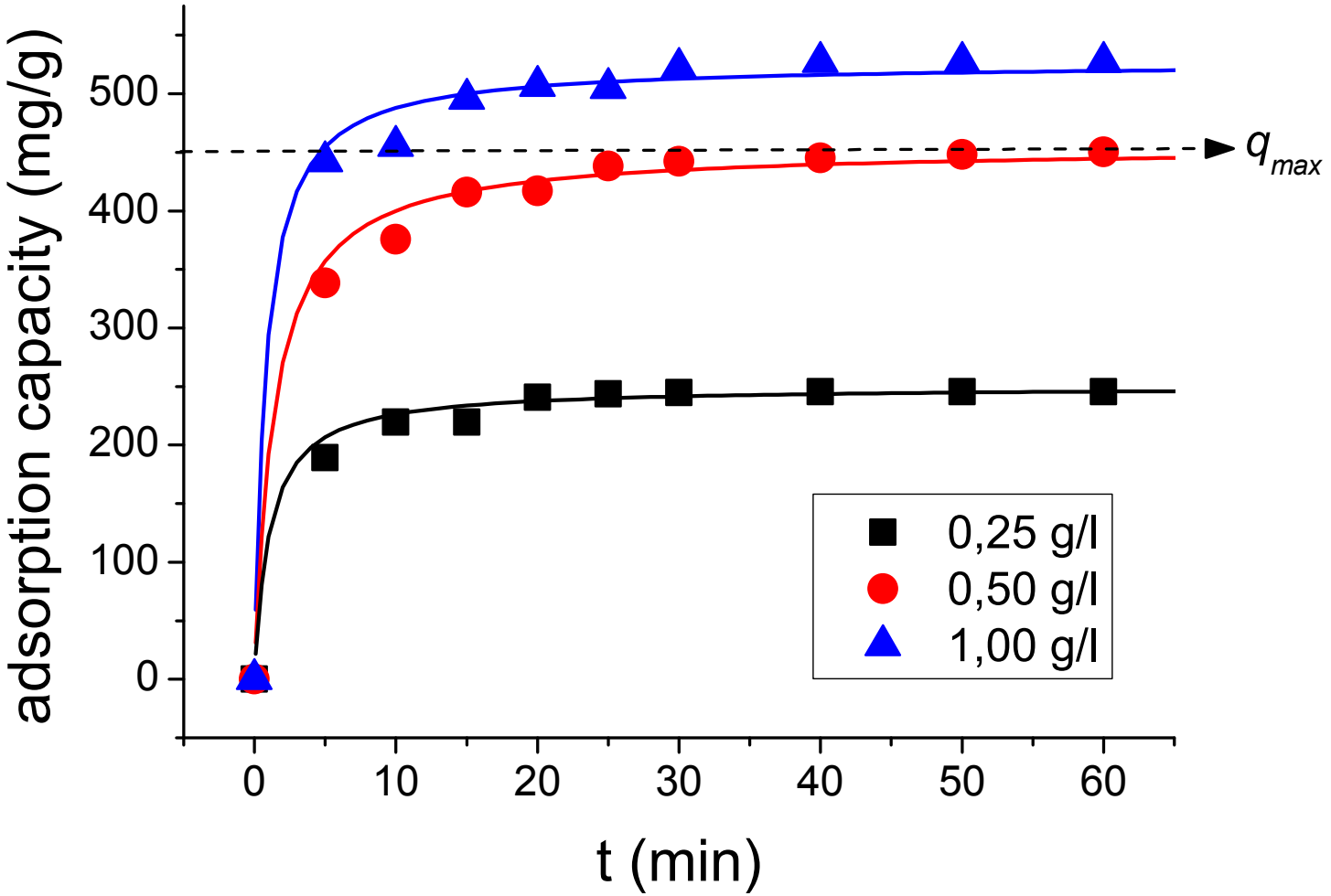
adsorption capacity (mg/g)
500
400
300
200
100
0
0
10
20
30
40
50
60
t (min)
q_{max}
0,25 g/l
0,50 g/l
1,00 g/l

Figure 4

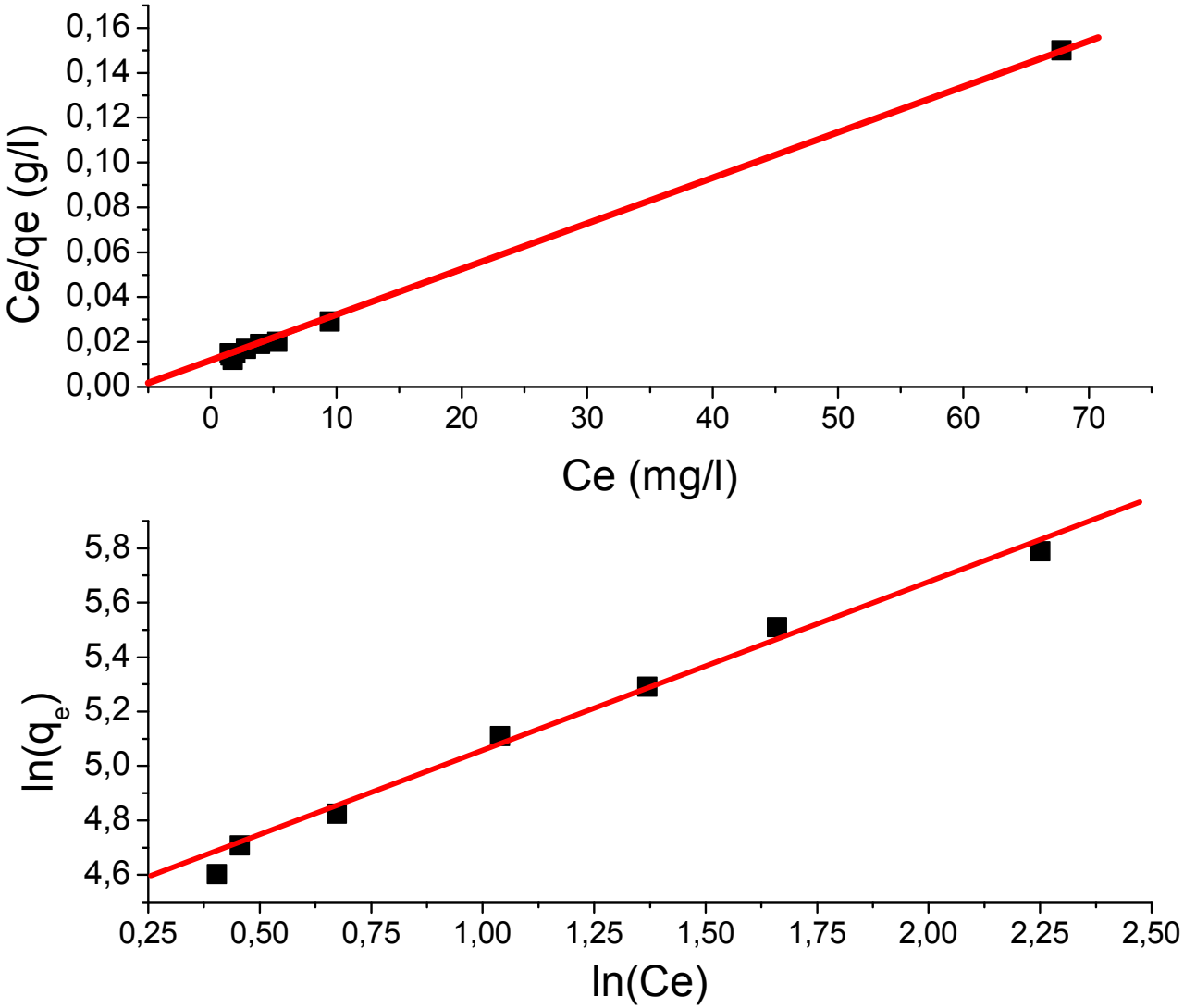
0,16
0,14
0,12
0,10
0,08
0,06
0,04
0,02
0,00
Ce/qe (g/l)
0
10
20
30
40
50
60
70
Ce (mg/l)
5,8
5,6
5,4
5,2
5,0
4,8
4,6
ln(qe)
0,25
0,50
0,75
1,00
1,25
1,50
1,75
2,00
2,25
2,50
ln(Ce)

Figure 5

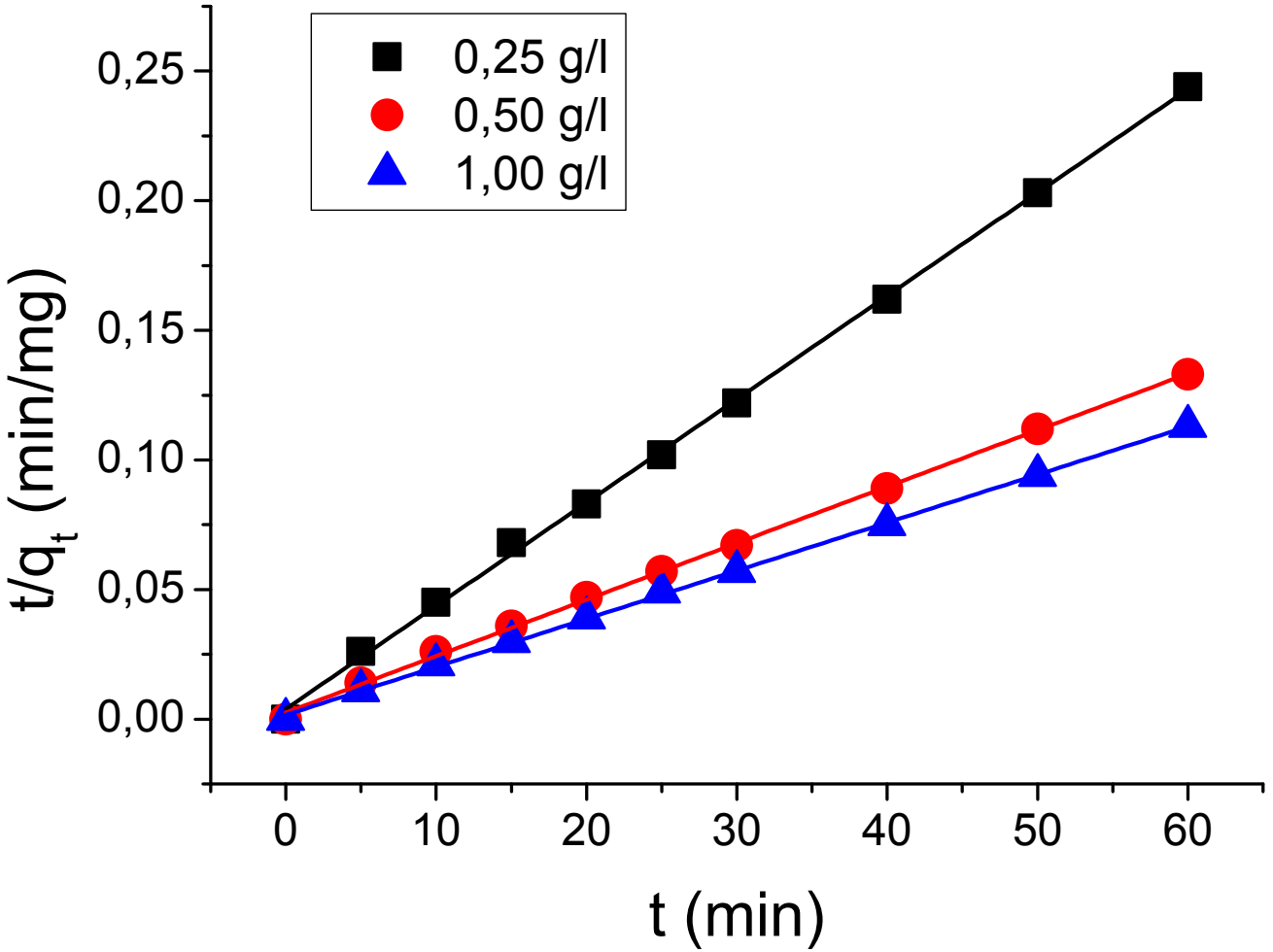
0,25 g/l
0,50 g/l
1,00 g/l
0,25
0,20
0,15
0,10
0,05
0,00
t/q_t (min/mg)
0
10
20
30
40
50
60
t (min)